Preprints of the 21st IFAC World Congress (Virtual)
Berlin, Germany, July 12-17, 2020

Experimentally Validated Sliding Mode Control of Multi-rotor UAV with Control Signal Constraints

Yuankang Zhu, Liuping Wang, Jyoti Mishra

School of Engineering, RMIT University, Melbourne, VIC 3000, Australia. (corresponding author: Liuping Wang; +61-3-9925-2100; e-mail: liuping.wang@rmit.edu.au)

Abstract: This paper proposes a cascade control strategy for multi-rotor unmanned aerial vehicle, where the inner-loop system is regulated by a sliding mode controller with disturbance observer and the outer-loop controller is a PID controller. Operational constraints are incorporated in the implementation for safety protection of the electronics. Experimental results are obtained to demonstrate the efficacy of the proposed design in comparison to a traditional cascade PID control system.

Keywords: unmanned aerial vehicle, disturbance observer, cascade control, operational constraints, sliding mode control.

1. INTRODUCTION

Nowadays, unmanned aerial vehicles (UAVs) have been increasingly developed in many applications such as remote data collection, filming, monitoring, and other civilian and military areas. Multirotor UAVs with more than four rotors, such as hexacopters and octocopters, are able to generate better flight stability with heavier payload than quadcopters in a general term. However, the main drawback with extra rotors is that the flight time is reduced due to the increase in drone size and weight. With the consideration of all the above-discussed facts, hexacopter is a good compromise between performance and flight time, see Alaimo et al. (2013).

In recent years, many control methods have been developed on multirotor UAVs, such as PID and LQR control, see Kuantama et al. (2018), Poksawat and Wang (2017), Wang (2020), model predictive control (MPC), see Ganga and Dharmana (2017) Ligthart et al. (2017) and many other linear control methods. Although there are more and more advanced linear control methods being proposed, PID is still widely popular in UAV applications due to its simplicity and practicality, see Mystkowski (2013). A self-tuning PID design has been introduced to reduce the design workload, see Babu et al. (2017). An auto-tuning design on a GPS-based antenna tracker has been proposed using Fuzzy PID logic, see Riyandi et al. (2018). A fuzzy-PI controller has been developed for autonomous moving target tracking, see Rabah et al. (2019). Due to the system's nonlinearity, nonlinear control methods have gained an increasing interest in recent years. Sumantri has developed a least square method based sliding mode control (SMC) for energy saving by chattering reduction, see Sumantri et al. (2016). Orosco has presented a parameter tuning method for SMC to improve the performance, see Orosco et al. (2018). Alkamachi has tried the mixed approach between the nonlinear SMC and linear PD control on overactuated quadcopter, see Alkamachi and Erçelebi (2019). However, all the aforementioned nonlinear control papers on UAVs are focused on the simulation results. Only a few papers have discussed the experimental results, see Elhennawy and Habib (2018) and see Garcia et al. (2019).

There are also many challenges during the multirotor controller design. The main purpose of the controller is to achieve the desired performance in order to satisfy user requirements. Due to several uncertainties problems including unknown actuators and sensor dynamics, varying nonlinear parameters and other measurement errors, it can be very difficult to build simulation platforms representing UAVs. Because of all these difficulties, a cascade control structure is introduced for attitude control together with automatic controller tuning strategies, which reduces the risk and the workload, see Tesch et al. (2016) and Wang (2020).

This paper differs from the existing control systems developed for the multi-rotor UAVs. It uses a cascade control system architecture, in which the inner-loop control system deploys sliding mode control with disturbance estimation that has been developed recently by the authors (Wang et al. (2019)), and the outer-loop control system utilizes a PID controller with an automatic tuning function. The advantages of the sliding mode control with disturbance estimation lead to a much faster inner-loop dynamic response in comparison to a traditional PID controlled system and an anti-windup mechanism for safety protection of the electronic components in the event of control signal exceeding its operational limits.

This rest of the paper is organized as follows. The mathematical model of a hexacopter is introduced in Section 2. Section 3 explains the cascaded control system with mixed SMC and PID controllers. Experimental results are discussed in Section 4. Section 5 concludes the research findings.

2. MODELLING OF HEXACOPTER

In this section, the mathematical model of hexacopter is represented. The hexacopter under study comprises of six individual rotors configured in 60 degrees apart. In order to maintain the balance of hexacopter, half of the rotors need to rotate in clockwise while the other halves have to rotate in the anti-clockwise direction, as shown in Figure 1.

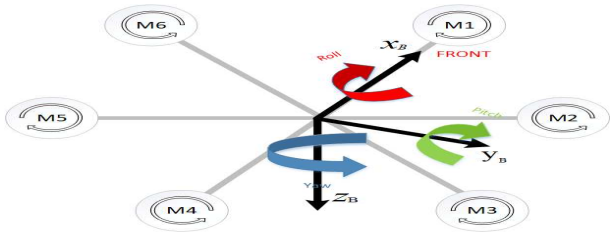

Fig. 1. Hexacopter Frame

where motors M_i $(i = 1, 2, 3, 4, 5, 6)$ will generate a total upward thrust vector against z axis. The hexacopter system also has six degrees of freedom (DOF) in 3 dimensions.

For the purpose of attitude control of a hexacopter, its dynamics consist of three subsystems: the subsystem for actuators, the subsystem based on body coordinate frame and the subsystem based on world coordinate frame.

Actuators

The input variables for the actuators are the directional torques τ_x, τ_y and τ_z along the x, y, z, and the output variables are the velocities of the six rotors (u_1, u_2, …, u_6). The relationships are determined by the solutions of the following linear equations:

$$\begin{bmatrix}\tau_x\\ \tau_y\\ \tau_z\end{bmatrix} = \overbrace{\begin{bmatrix} 0 & \frac{1}{2}\sqrt{3}l & \frac{1}{2}\sqrt{3}l & 0 & -\frac{1}{2}\sqrt{3}l & -\frac{1}{2}\sqrt{3}l \\ -l & -\frac{1}{2}l & \frac{1}{2}l & l & \frac{1}{2}l & -\frac{1}{2}l \\ d & -d & d & -d & d & -d \end{bmatrix}}^{\Phi} \begin{bmatrix}u_1\\ u_2\\ u_3\\ u_4\\ u_5\\ u_6\end{bmatrix}, \quad (1)$$

where l is the distance from the Center-of-Gravity of the UAV to the motors, and d is the drag coefficient. Clearly the subsystem for the actuators has only steady-state relations. When the dynamics (1) are investigated, it is found that the average motor force that is imposed by the motors does not influence the sum of torques that act on the hexacopter's body. For example, increasing all motor forces does not affect the hexacopter's attitude behaviour when the hexacopter is designed with a balanced structure. For that reason, Equation (1) can be rewritten as,

$$\begin{bmatrix}\tau_x\\ \tau_y\\ \tau_z\end{bmatrix} = \Phi \left(\begin{bmatrix}u_1\\ \vdots\\ u_6\end{bmatrix} - \begin{bmatrix}v_i\\ \vdots\\ v_i\end{bmatrix} \right) \triangleq \Phi \begin{bmatrix}\bar{u}_1\\ \vdots\\ \bar{u}_6\end{bmatrix}, \quad (2)$$

in which $v_i = \frac{\sum_{i=1}^{6} u_i}{6}$ such that,

$$\sum_{i=1}^{6} \bar{u}_i = 0. \quad (3)$$

When the hexacopter's dynamics are investigated even more thoroughly, it is seen that the two motors in the so-called motor pairs $(1, 4)$, $(2, 5)$, and $(3, 6)$ impose opposite body torques in all direction. The motors in each motor pair are located at opposite sides of the hexacopter. Therefore, only the difference in force between each of these two motors has an effect on the hexacopter's attitude behaviour. For that reason, it is useful to impose the following relation for the motor forces,

$$\begin{aligned}\bar{u}_1 &= -\bar{u}_4\\ \bar{u}_2 &= -\bar{u}_5\\ \bar{u}_3 &= -\bar{u}_6.\end{aligned} \quad (4)$$

With this definition, the total motor force can be defined independently from the attitude behaviour. Therefore, the motor forces can be controlled as such that these are on average at an optimal distance from their saturation boundary. This increases the hexacopter's stability especially during intense manoeuvring.

By substituting the motor speed constraints proposed by (4) into (2), we obtain the relationships for actuators are described by the linear equations (Ligthart et al. (2017)),

$$\begin{bmatrix}\tau_x\\ \tau_y\\ \tau_z\end{bmatrix} = \begin{bmatrix} 0 & \sqrt{3}l & \sqrt{3}l \\ -2l & -l & l \\ 2d & -2d & 2d \end{bmatrix} \overbrace{\begin{bmatrix}\bar{u}_1\\ \bar{u}_2\\ \bar{u}_3\end{bmatrix}}^{\hat{u}}. \quad (5)$$

For calculation of the rotors' speed, once the control signals τ_x, τ_y and τ_z determined, the following equation is used,

$$\begin{bmatrix}\bar{u}_1\\ \bar{u}_2\\ \bar{u}_3\end{bmatrix} = \begin{bmatrix} 0 & \sqrt{3}l & \sqrt{3}l \\ -2l & -l & l \\ 2d & -2d & 2d \end{bmatrix}^{-1} \begin{bmatrix}\tau_x\\ \tau_y\\ \tau_z\end{bmatrix} \quad (6)$$

For safety protection, a maximum rotor speed u^{max} is imposed in the attitude control problem, which, in turn, is converted into the maximum values for τ_x, τ_y and τ_z via equation (5). As a result, the following operational constrains are imposed for the variables $\tau_x^{max} = 2\sqrt{3}lu^{max}$, $\tau_y^{max} = -2lu^{max}$ and $\tau_z^{max} = 2du^{max}$.

Subsystem based on the body coordinate frame

The input signals for the subsystem based on the body coordinate frame are τ_x, τ_y and τ_z and the output signals are rotational velocities, p, q and r in the body coordinate frame. The dynamic relationship is governed by the following differential equations:

$$\begin{bmatrix}\dot{p}\\ \dot{q}\\ \dot{r}\end{bmatrix} = \begin{bmatrix}(I_{yy} - I_{zz})qr/I_{xx}\\ (I_{zz} - I_{xx})pr/I_{yy}\\ (I_{xx} - I_{yy})pq/I_{zz}\end{bmatrix} + \begin{bmatrix}\tau_x/I_{xx}\\ \tau_y/I_{yy}\\ \tau_z/I_{zz}\end{bmatrix}. \quad (7)$$

where I_{xx}, I_{yy} and I_{zz} stand for the inertial moments about x, y and z axes. It is clearly seen that these are bilinear systems.

Subsystems based on the world coordinate frame

This is the coordinate frame with variables that define the attitude of a hexacopter. The input signals to the subsystems are the rotational velocities, p, q and r in the body coordinate frame, and the output signals are three Euler angles: roll ϕ, pitch θ and yaw ψ. The mapping of between the input and output variables is given the following differential equations:

$$\begin{bmatrix}\dot{\phi}\\ \dot{\theta}\\ \dot{\psi}\end{bmatrix} = \overbrace{\begin{bmatrix} 1 & \sin(\phi)\tan(\theta) & \cos(\phi)\tan(\theta) \\ 0 & \cos(\phi) & -\sin(\phi) \\ 0 & \sin(\phi)/\cos(\theta) & \cos(\phi)/\cos(\theta) \end{bmatrix}}^{R_{RPY}} \begin{bmatrix}\mathrm{p}\\ \mathrm{q}\\ \mathrm{r}\end{bmatrix}$$

Attitude control
For attitude control of an unmanned aerial vehicle, the outputs are the roll and pitch Euler angles and yaw angular velocity, ϕ, θ and r respectively. The control objective is that for given reference signals ϕ^*, θ^* and r^*, the roll, pitch Euler angles and yaw rate will follow their respective reference signals and reject disturbances caused by turbulence and the payload of the UAV. The maintain stable flight, the common reference signals are chosen to be $\phi^* = 0$ and $\theta^* = 0$ while r^* is manually determined and transmitted through a remote transmitter.

Cascade control structure
The three subsystems mentioned above naturally yield to the choice of cascade control structure for the hexcopter. Figure 2 shows the cascade control structure used in this paper. From this figure, it is seen that the outer-loop control system achieves the final control objective with two PID controllers to generate the control signals, which are also the reference signals to the inner-loop systems p^* and q^*. Together with r^*, three sliding mode controllers with disturbance observer are used to generate the control signals τ_x, τ_y and τ_z. With the relationship between the rotor speed and the control signals τ_x, τ_y and τ_z, the reference signals to the first three rotors are calculated based on the linear equations described by (6), and the rest of the three rotors' speed equals to the first three but with an opposite sign.

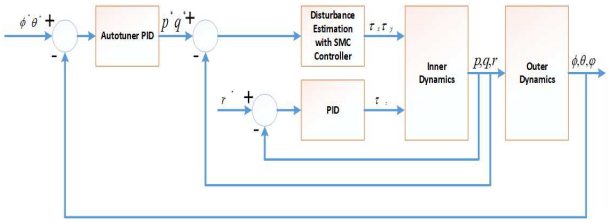

Fig. 2. Cascaded Attitude Control Structure

3. INNER-LOOP AND OUTER-LOOP CONTROL SYSTEM DESIGN

This section describes the cascaded control configuration of the attitude control system, as shown in Figure. Furthermore, from (7), it is clearly seen that the inner-loop has coupled nonlinearity and integrator dynamics. In order to stabilize the hexacopter, a mixed PID and SMC cascaded structure is chosen. The inner-loop controls the angular rates by using an improved SMC controller to deal with the system nonlinearity while the outer-loop controls the Euler angles by choosing an autotuned PID method.

3.1 Angular Rates Loop Design

Due to the cascaded control configuration, the reference signal to the inner-loop controller is the control signal of the outer-loop controller and the feedback signal is directly coming from the inner-loop output signal, as shown in Figure 2. Comparing with the traditional PID controller, the proposed SMC controller with estimated observer design is more robust in handling the system nonlinearities, unknown factors and disturbances, see Wang (2020). Because of the symmetric structure in hexacopter, the controller parameters of roll and pitch angles can be the same.

In order to design the SMC controller, the differential equation of Euler angle ϕ can be expressed as,

$$\dot{\phi}(t) = b(u_\phi(t) + d_\phi(t)) \tag{8}$$

where $u_\phi(t)$ and $\phi(t)$ are input and output variables, $b = \frac{1}{I_{xx}}$ depends on hexacopter, and $d_\phi(t)$ is the disturbance. Here, the linearization of the nonlinear model (7) leads to the integral linear model (8). Assuming that disturbance $d_\phi(t)$ is a constant turbulence, we have:

$$\dot{d_\phi}(t) = 0$$

Assuming the first order SMC control equation is,

$$\tilde{u}_\phi(t) = -K_1 sign\phi(t) \tag{9}$$

where $K_1 > 0$, $\tilde{u}_\phi(t) = u_\phi(t) + d_\phi(t)$.

Since the hexacopter has coupled nonlinear dynamics, a first-order SMC controller is not able to deal with all unknown parts without having input saturation. Therefore, it is necessary to design an extra observer to estimate and compensate these nonlinearities in order to make the magnitude of the controller output smaller. The disturbance dynamics can be written as follows by rearranging (8),

$$bd_\phi(t) = \dot{\phi}(t) - bu_\phi(t). \tag{10}$$

Let us define the estimated disturbance signal as $\hat{d}_\phi(t)$. The error between $d_\phi(t)$ and $\hat{d}_\phi(t)$ can be expressed as,

$$\varepsilon_\phi(t) = bd_\phi(t) - b\hat{d}_\phi(t) = \dot{\phi}(t) - bu_\phi(t) - b\hat{d}_\phi(t). \tag{11}$$

The unknown disturbance $d_\phi(t)$ can be estimated by the proposed observer as,

$$\frac{d\hat{d}_\phi(t)}{dt} = K_2(\dot{\phi}(t) - bu_\phi(t) - b\hat{d}_\phi(t)) \tag{12}$$

where the observer gain $K_2 = \frac{\alpha_2}{b}$ is selected to ensure the convergence of the disturbance estimation error

$$\tilde{d_\phi}(t) = d_\phi(t) - \hat{d_\phi}(t) \tag{13}$$

Now, the control signal is computed using,

$$u_\phi(t) = -K_1 sign\phi(t) - \hat{d}_\phi(t). \tag{14}$$

To implement the proposed algorithm to the hexacopter, there is a derivative term in the equation of output signal, as shown in (12). In order to eliminate this term, an intermediate variable $\hat{z}_\phi(t)$ is defined as,

$$\hat{z}_\phi(t) = \hat{d}_\phi(t) - K_2\phi(t). \tag{15}$$

As Wang (2020), the computation of the disturbance estimation becomes:

$$\begin{aligned}&\hat{z}_\phi(t_{i+1}) = \\ &\quad \hat{z}_\phi(t_i) - (K_2 b\hat{z}_\phi(t_i) + K_2^2 b\phi(t_i) + K_2 bu_\phi(t_i))\Delta t.\end{aligned} \tag{16}$$

Finally, the estimated disturbance signal at sample t_i becomes

$$\hat{d}_\phi(t_i) = \hat{z}_\phi(t_i) + K_2(\phi(t_i) - \phi^*(t_i)). \tag{17}$$

Then, the control signal equation can be written by

$$u_\phi(t_i) = -K_1 sign(\phi(t_i) - \phi^*(t_i)) - \hat{d}_\phi(t_i) \tag{18}$$

while $\hat{d}_\phi(t_{i+1})$ need to be updated in each sample.

Because the integral action is introduced through the estimation of a constant, constraints can be naturally incorporated in the implementation of the sliding mode control.

3.2 Outer-Loop Controller Design

Once the inner-loop sliding mode controllers are implemented, the outer-loop PID controllers are to be designed. The parameters to be determined for a PID controller are the proportional control gain K_c, the integral time constant, τ_I and derivative gain τ_D. These parameters are auto-tuned using the auto-tuner presented in Wang (2020) and the implementation of the controllers is performed using velocity discrete-time form with anti-windup mechanism. More details of the auto-tuner and the implementation can be found in Wang (2020).

An experimental feedback relay test is designed for hexacopter so that the input and output data can be collected to estimate its dynamics. Because the outer-loop system has integrating dynamics, a known gain K_t is chosen to maintain the overall stability such that the system output exhibits a sustained oscillation. Figure 6 shows the testing results of the relay control system.

The closed-loop frequency response can be approximated by the input and output data obtained from the relay test as,

$$T(j\omega_1) = \frac{K_t G(j\omega_1)}{1 + K_t G(j\omega_1)} \tag{19}$$

where $G(j\omega_1)$ is the open-loop frequency response at the fundamental frequency ω_1. A Fourier transform analysis can be applied here. According to (19), the closed-loop frequency response $T(e^{j\omega})$ can be expressed as,

$$T(e^{j\omega}) = \frac{1}{K_t} \frac{T(e^{j\omega})}{1 - T(e^{j\omega})} \tag{20}$$

where $\omega = 2\pi/T$ and T is the oscillation time period.

Assuming the outer-loop system dynamics equal to an integrating function with a time delay model, we can write

$$G(s) = \frac{K_p e^{-ds}}{s} \tag{21}$$

where,

$$\begin{aligned} K_p &= \omega \left| G(j\omega) \right| \\ d &= -\frac{1}{\omega} tan^{-1} \frac{Image(jG(j\omega))}{Real(jG(j\omega))}. \end{aligned} \tag{22}$$

Those two coefficients are used to calculate the PID controller parameters, see Wang.L (2000). The desired controller parameters are computed by the specified phase margin and gain margin as,

$$\begin{aligned} K_c &= \frac{\hat{K}_c}{dK_p} \\ \tau_I &= \hat{\tau_I} d \\ \tau_d &= \hat{\tau_d} d \end{aligned}$$

In addition,

$$\begin{aligned} \hat{K_c} &= \frac{1}{0.5080\beta + 0.6208} \\ \hat{\tau_I} &= 1.9885\beta + 1.2235 \\ \hat{\tau_D} &= \frac{1}{1.0043\beta + 1.8194} \end{aligned} \tag{23}$$

where β is the performance parameter that leads to the desired time constant as βd, phase margin and gain margin of the system, see Wang (2020).

4. EXPERIMENTAL RESULTS

The hexacopter onboard microcontroller is operated with a sampling interval of $\Delta t = 0.008$(sec). Firstly, the inner-loop system is operated with the improved SMC controller, followed by the outer-loop autotuned PID. Due to the symmetrical structure of the hexacopter, roll and pitch axis are allowed to share the same controller parameters. A comparison study will be performed under the extra wind turbulence between the proposed method and the traditional cascade PID control method. All input references are programmed as groups of step-change signals including roll, pitch, and yaw.

4.1 Angular Rate Loop

In Comparison to the traditional PID controllers for the inner-loop system, the proposed SMC controllers are more robust for handling the system nonlinearity and minimizing the design workload. The controller gain (K_1) of roll and pitch axes are selected as 0.5. The observer gain (K_2) is chosen as 0.2. As mentioned before, the yaw axis does not have an outer-loop. The SMC and observer gains of yaw axis are $K_1^{yaw} = 2.44$ and $K_2^{yaw} = 0.92$. According to Figure (3)-(5), the inner-loop is perfectly tracking its reference.

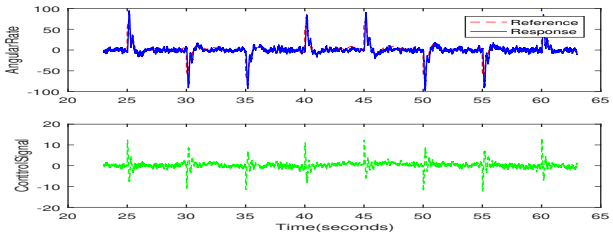

Fig. 3. The Response of Roll Rate with SMC controller

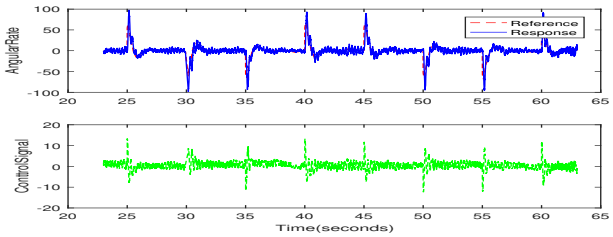

Fig. 4. The Response of Pitch Rate with SMC controller

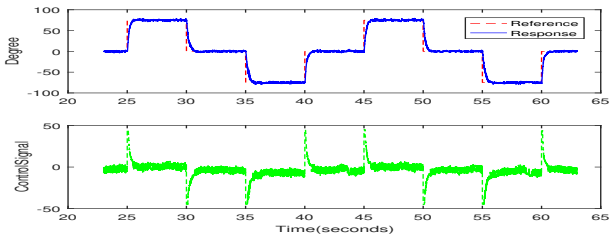

Fig. 5. The Response of Yaw Angle with SMC controller

4.2 Outer Loop Control System

Once the inner-loop is tuned, the outer-loop controller parameters are selected by an automatic tuning method.

For the inner-loop feedback relay test, a known gain K_t is selected as 1 and the relay amplitude value is selected as 30 degrees ($\epsilon = 30$). The amplitude of hysteresis has to be smaller than the value of relay amplitude, therefore, it has been chosen as half of the relay amplitude.

The input and output sustained oscillation are shown in Figure 6

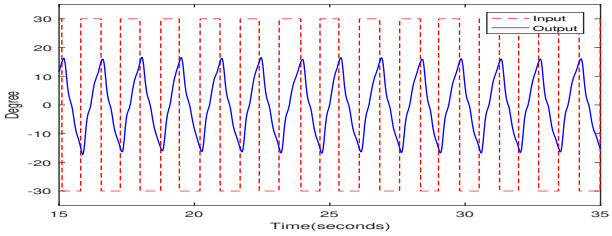

Fig. 6. Outer Loop Relay Test

The closed-loop frequency response is calculated from the estimated data

$$T(e^{j\omega_1}) = -0.1029 - 0.3324i$$

where the fundamental frequency $\omega_1 = 2\pi/(N\Delta t)$. Then the estimated frequency response of the outer-loop is

$$T(e^{j\omega}) = 0.0198 - 0.3631i.$$

We obtained the estimated outer-loop dynamics equation as

$$G(s) = \frac{0.9675e^{-0.108s}}{s}.$$

Based on (22), it is very easy to calculate the outer loop controller parameters, such as $K_c = 3.61$, $\tau_I = 0.2$, and $\tau_D = 0.0019$.

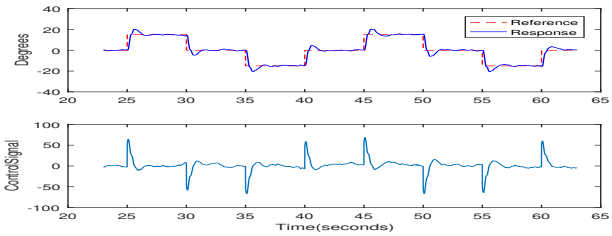

Fig. 7. The Response of Roll Angle

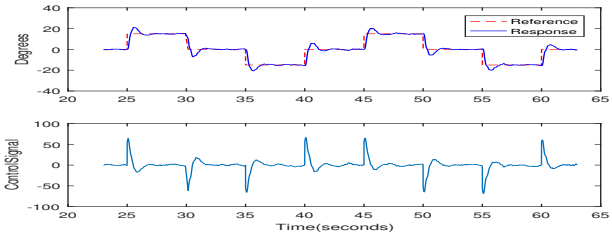

Fig. 8. The Response of Pitch Angle

From Figure 8 and Figure 7, it is obviously seen that the hexacopter is capable of following the desired reference signals. Those overshoot parts are produced by a programmed rapidly step change which supposes be the way slower in manual operating conditions. In addition, the three Euler angles are able to maintain their stability during the real flight test.

Table 1. MSE with different controllers

Controllers	Attitude Angles (MSE)
Proposed Method	9.1661
Traditional PID	21.4221

4.3 Comparison Study Under External Wind Turbulence

The mean squared error(MSE) values are evaluated with the performance of the proposed control algorithm. The external wind turbulence is generated by a high-velocity floor fan in which the rotating speed is 1350 RPM. The input reference signal is programmed with anti-windup constraints at 15 degrees. The MSE values are calculated from the following form,

$$MSE = \frac{1}{n}\sum_{1}^{n}(Response - Reference)^2 \qquad (24)$$

where n is the data length.

The proposed method includes an improved SMC controller in the inner loop and an automatic tuning PID controller in the outer loop while the traditional PID has a cascaded PID controller.

Table. 1 represents the MSE values of the proposed method and the traditional PID method. Table. 2 represents the corresponding the controller gain values. It is also clearly seen that the proposed method is tracking the reference signal better than traditional PID, as shown in Figure 9. According to Table. 1 and Figure 9, this proposed method is much stronger than the traditional PID in the presence of external wind turbulence.

Table 2. Controller Parameters

Proposed Method	Traditional PID
$K_1 = 0.5$	$K_c^{in} = 0.11$
$K_2 = 0.2$	$\tau_I^{in} = 0.65$
$K_c = 3.61$	$\tau_d = 0.009$
$\tau_I = 0.2$	$K_c^{out} = 1.9$
$\tau_d = 0.0019$	$\tau_I^{out} = 0.7037$
nan	$\tau_d^{out} = 0.0526$

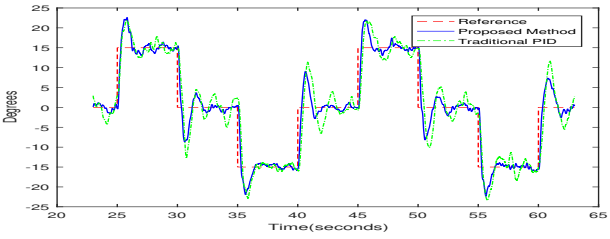

Fig. 9. Controller Comparison

4.4 Gain Variations

In the SMC control with disturbance observer, there are five cases of K_1 applied in the inner-loop controller varying from 0.2 to 0.8 as shown in Table. 3. From Table. 3, the hexacopter is generated the smallest MSE value ($MSE = 9.1661$) when $K_1 = 0.5$.

5. CONCLUSION

This paper discusses a mixed approach that consists of an improved SMC controllers and autotuned PID controllers

Table 3. Controller Gain Variations

SMC Gains	Attitude Angles (MSE)
$K_1 = 0.8$	9.7441
$K_1 = 0.6$	9.3796
$K_1 = 0.5$	9.1661
$K_1 = 0.4$	9.9129
$K_1 = 0.2$	10.0205

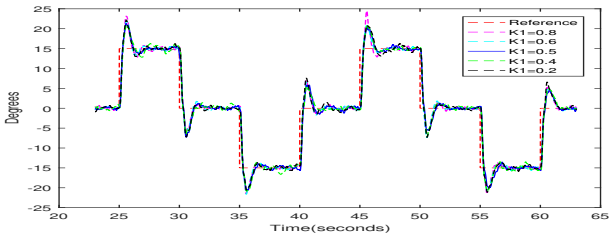

Fig. 10. Gain Comparison

where the disturbance observer implementation and experimental relay test are demonstrated. Experimental results have shown that the proposed method stabilizes the hexacopter with attitude tracking.

REFERENCES

Alaimo, A., Artale, V., Milazzo, C., Ricciardello, A., and Trefiletti, L. (2013). Mathematical modeling and control of a hexacopter. *2013 International Conference on Unmanned Aircraft Systems, ICUAS 2013 - Conference Proceedings*, 1043–1050. doi: 10.1109/ICUAS.2013.6564793.

Alkamachi, A. and Erçelebi, E. (2019). A proportional derivative sliding mode control for an overactuated quadcopter. *Proceedings of the Institution of Mechanical Engineers, Part G: Journal of Aerospace Engineering*, 233(4), 1354–1363. doi:10.1177/0954410017751739.

Babu, V.M., Das, K., and Kumar, S. (2017). Designing of self tuning PID controller for AR drone quadrotor. *2017 18th International Conference on Advanced Robotics, ICAR 2017*, (July), 167–172. doi: 10.1109/ICAR.2017.8023513.

Elhennawy, A.M. and Habib, M.K. (2018). Nonlinear robust control of a quadcopter: Implementation and evaluation. *Proceedings: IECON 2018 - 44th Annual Conference of the IEEE Industrial Electronics Society*, 1, 3782–3787. doi:10.1109/IECON.2018.8591344.

Ganga, G. and Dharmana, M.M. (2017). MPC controller for trajectory tracking control of quadcopter. *Proceedings of IEEE International Conference on Circuit, Power and Computing Technologies, ICCPCT 2017*. doi:10.1109/ICCPCT.2017.8074380.

Garcia, O., Ordaz, P., Santos-Sanchez, O.J., Salazar, S., and Lozano, R. (2019). Backstepping and Robust Control for a Quadrotor in Outdoors Environments: An Experimental Approach. *IEEE Access*, 7, 40636–40648. doi:10.1109/ACCESS.2019.2906861.

Kuantama, E., Tarca, I., and Tarca, R. (2018). Feedback Linearization LQR Control for Quadcopter Position Tracking. *2018 5th International Conference on Control, Decision and Information Technologies, CoDIT 2018*, 204–209. doi:10.1109/CoDIT.2018.8394911.

Ligthart, J.A., Poksawat, P., Wang, L., and Nijmeijer, H. (2017). Experimentally validated model predictive controller for a hexacopter. *IFAC-PapersOnLine*, 50(1), 4076–4081.

Mystkowski, A. (2013). Robust control of the micro UAV dynamics with an autopilot. *Journal of Theoretical and Applied Mechanics*, 51(3), 751–761.

Orosco, V., Chavez, D., Camacho, O., and Aguilar, J. (2018). Algorithms. *2018 IEEE Third Ecuador Technical Chapters Meeting (ETCM)*, 1–6.

Pakorn, P. Liuping, Wang (2017). Automatic tuning of hexacopter attitude control systems with experimental validation. *2017 21st International Conference on System Theory, Control and Computing, ICSTCC 2017*, 753–758. doi:10.1109/ICSTCC.2017.8107127.

Rabah, M., Rohan, A., Mohamed, S.A., and Kim, S.H. (2019). Autonomous Moving Target-Tracking for a UAV Quadcopter Based on Fuzzy-PI. *IEEE Access*, 7, 38407–38419. doi:10.1109/ACCESS.2019.2906345.

Riyandi, A., Sumardi, S., and Prakoso, T. (2018). PID Parameters Auto-Tuning on GPS-based Antenna Tracker Control using Fuzzy Logic. *Jurnal Teknologi dan Sistem Komputer*, 6(3), 122. doi: 10.14710/jtsiskom.6.3.2018.122-128.

Sumantri, B., Uchiyama, N., and Sano, S. (2016). Least square based sliding mode control for a quad-rotor helicopter and energy saving by chattering reduction. *Mechanical Systems and Signal Processing*, 66-67, 769–784. doi:10.1016/j.ymssp.2015.05.013. URL `http://dx.doi.org/10.1016/j.ymssp.2015.05.013`.

Tesch, D.A., Eckhard, D., and Guarienti, W.C. (2016). Pitch and Roll control of a Quadcopter using Cascade Iterative Feedback Tuning. *IFAC-PapersOnLine*, 49(30), 30–35. doi:10.1016/j.ifacol.2016.11.118. URL `http://dx.doi.org/10.1016/j.ifacol.2016.11.118`.

Wang, L. (2020). *PID Control System Design and Automatic Tuning using MATLAB/Simulink*. Wiley-IEEE PRESS.

Wang, L., Mishra, J., Zhu, Y., and Yu, X. (2019). An improved sliding mode current control of induction machine in presence of voltage constraints. *IEEE Transactions on Industrial Informatics*, PP, 1–1. doi: 10.1109/TII.2019.2944228.

Wang.L, Taylor Francis. (2000). *From Plant Data to Process Control: Ideas for Process Identification and PID Design*.